From the Hopf bifurcation to fully developed turbulence in incompressible flows

C. H. Bruneau[1],

Summary

The first bifurcations in 2D lid-driven cavity flows are first studied. Then turbulent flows are simulated in the cavity and behind arrays of cylinders in a channel. They confirm on the one hand the presence of an attractor and on the other hand the coexistence of both direct enstrophy and inverse energy cascades.

Introduction

The aim of this work is to study the stability and the behaviour of incompressible flows at high Reynolds numbers. The first step is the loss of stability of the steady solution when the first Hopf bifurcation occurs. It is carefully computed on the square lid-driven cavity problem by computing the first Lyapunov exponent and the results are in good agreement with the few results available in the literature. Then, we try to localize the second bifurcation when several frequencies become active. Finally, fully developed turbulent flows are computed. Still in the cavity, the solutions computed with two different initial data confirm the existence of an attractor. In addition to this academic test case, we compute turbulent flows in a channel behind arrays of cylinders. This numerical simulation corresponds to soap film experiments and the results are in good agreement with the one observed. In particular, we show the coexistence of the direct enstrophy cascade and an inverse energy cascade which slope is very close to $k^{-5/3}$.

First bifurcations

In this section, we study the stability of the first branches of solutions for the lid-driven cavity problem on a square domain $\Omega = (0,1) \times (0,1)$. The unsteady Navier-Stokes equations read :

$$\left\{ \begin{array}{rcll} \partial_t U - \dfrac{1}{Re}\Delta U + (U.\nabla)U + \nabla p & = & 0 & \text{in }]0,T[\times\Omega \\ \nabla.U & = & 0 & \text{in }]0,T[\times\Omega \end{array} \right. \tag{1}$$

where $U = (u,v)$ is the velocity, p is the pressure and T is the simulation time. These equations are coupled to an initial datum $U(0,x,y) = U_0(x,y)$ in Ω and relevant boundary conditions (BC). Namely no-slip BC on the walls, non homogeneous Dirichlet BC for the constant lid in the cavity or the incoming Poiseuille flow in the channel and non-reflecting BC at the artificial frontier downstream in the channel [4].

At low Reynolds numbers (Re), we can study the stability of the steady solutions (U_S, p_S) of system (1) by computing the first Lyapunov exponent. We assume that a small

[1]MAB, Université Bordeaux 1, 33504 Talence, France

perturbation (V,q) is added to the steady solution and observe the behaviour of this perturbation along time. This behaviour is driven by the smallest real part of the eigenvalues of the linearized space operator. If the steady solution is stable, the perturbation goes to zero when t goes to infinity as $e^{\mu_1 t}$ where μ_1 is the first Lyapunov exponent defined by (see [2]):

$$\mu_1 = \lim_{t \longrightarrow +\infty} \frac{\mathrm{Log}\|V(t)\|}{t}. \tag{2}$$

Using the fact that (U_S, p_S) is a steady solution, we can solve only the simplified linear problem:

$$\left\{ \begin{array}{rcll} \partial_t V - \dfrac{1}{Re}\Delta V + (U_S \cdot \nabla)V + (V \cdot \nabla)U_S + \nabla q &=& 0 & \text{in }]0,T[\times\Omega \\ \nabla \cdot V &=& 0 & \text{in }]0,T[\times\Omega \\ V &=& V_0 & \text{in } \Omega \\ V &=& 0 & \text{on }]0,T[\times\partial\Omega \end{array} \right. \tag{3}$$

where the nonlinear term $(V \cdot \nabla)V$ is neglected. The evolution of the Lyapunov exponent versus the Reynolds number is given in table(1). It shows that the first Hopf bifurcation occurs around $Re = 8000$. These results are confirmed on the one hand by computation of the first eigenvalues of the linearized problem which gives a critical Reynolds number $R_c = 7998.5$ in [6] and $R_c = 8031.93$ in [9], and on the other hand by numerical simulations, in particular $R_c = 8018$ in [3]. In addition, at $Re = 8050$ it is not possible to get a steady solution. The solution computed directly from equations (1) is purely periodic with a frequency $f = 0.45$. This value is in complete agreement with the results obtained in [3] as they indicate that the frequency just beyond R_c is $0.42 \leq f \leq 0.48$. Our conclusion is that $8000 \leq R_c \leq 8050$. Then, we explore the second branch solution for higher Reynolds

Re	10	100	1000	5000	7800	8000
T	38	110	242	1386	2243	7442
μ_1	-5.2	-0.56	-0.076	-0.013	-0.0082	-0.0026

Table 1: Evolution of the Lyapunov exponent with Reynolds number.

numbers. The solution remains purely periodic for a wide range of Reynolds numbers but at $Re = 10000$ it seems that there are some tiny fluctuations in the signal obtained at a monitoring point on a very fine grid 2048×2048. Indeed, if we observe carefully such a signal on figure 1 we see that, in addition to the main periodic signal of period approximately equal to 1.65, there is a big pattern corresponding to these fluctuations which is reproduced for instance from times $t \approx 40$ to $t \approx 51$ and from times $t \approx 51$ to $t \approx 62$. This pattern corresponds a priori to the addition of another periodic phenomenon with a period around 11. But, if we select an entire number of these patterns and perform a Fourier analysis, we see that the spectrum reveals three frequencies. The main frequency $f_1 = 0.61$ gives a peak of huge amplitude but there are two more peaks of lower frequencies $f_2 = 0.175$

and $f_3 = 0.4375$ and small amplitude. In addition we can see in the spectrum some harmonics of these three frequencies. The Fourier analysis seems to be in contradiction with the observations on the signal but is not as these two frequencies are commensurate and equal respectively to twice and five times 0.0875. This last value corresponds to the period observed on the signal. In the literature, there are very few results on the second branch and some authors still find a steady solution at $Re = 10000$! In two recent papers, there are some results on this that validate the presence of a second branch around $Re = 10000$, in [3] at $Re = 9765$ and in [8] at $Re = 10300$. Nevertheless the frequencies obtained are very different, in the first paper they found $f_1 = 0.45$ and $f_2 = 0.2736$, in the second paper they found $f_1 = 0.0017$ and $f_2 = 0.069$. Thus it is difficult to conclude. In [3], they found that the frequency of the first branch $f_1 = 0.45$ is conserved in the second branch obtained when a second incommensurate frequency becomes active. In the present work, we find that the main frequency has changed and there is two additional frequencies. The question is still open and we can imagine many scenarios, for instance that there are two branches very close to each other, the second one corresponding to the description in [3] and the third one corresponding to the description above.

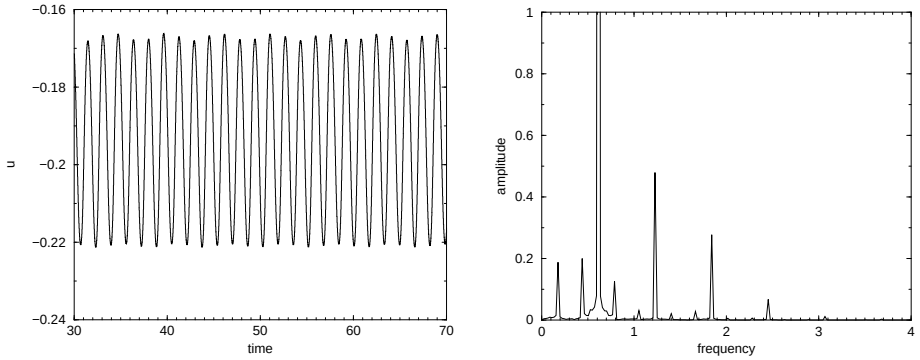

Figure 1: Horizontal velocity history (left) and power spectrum (right) at monitoring point (14/16,1/16) for $Re = 10000$ on grid 2048×2048.

Turbulent flows

We start this section with computations at high Reynolds number $Re = 100000$ in the cavity. The goal is to study the behaviour of the turbulent solution with respect to the initial datum. So, we perform one simulation starting from rest and another simulation initializing by the stable steady solution obtained at $Re = 5000$. We show on figure 2 the evolution of the global quantities energy and enstrophy. At time $t = 0$ the energy is $E = 0$ and increases for the first simulation while it starts from $E = 4.73 \times 10^{-2}$ and decreases for the second. Both curves seem to go to the same asymptotic state. In the meantime, the enstrophy histories which are very different at the beginning converge to each other. This confirms the presence of an attractor for Navier-Stokes equations in 2D as we can see that the final stages are very similar. Indeed, if we analyze the signals at the end of the simulations at a monitoring point, we get about the same spectra (figure 3).

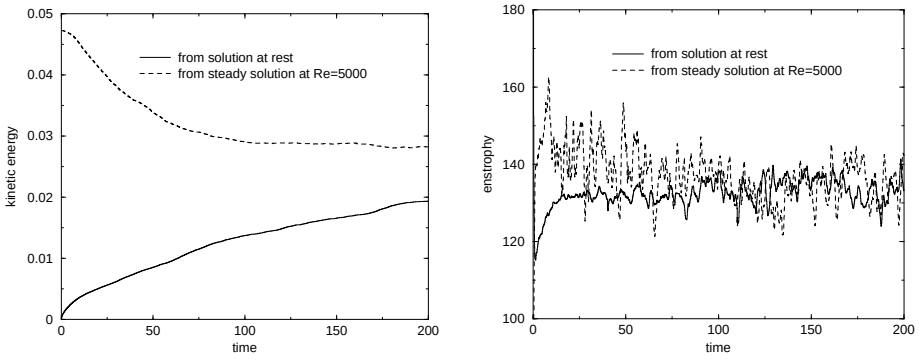

Figure 2: Comparison of the energy (left) and the enstrophy (right) histories at $Re = 100000$ with the two initializations.

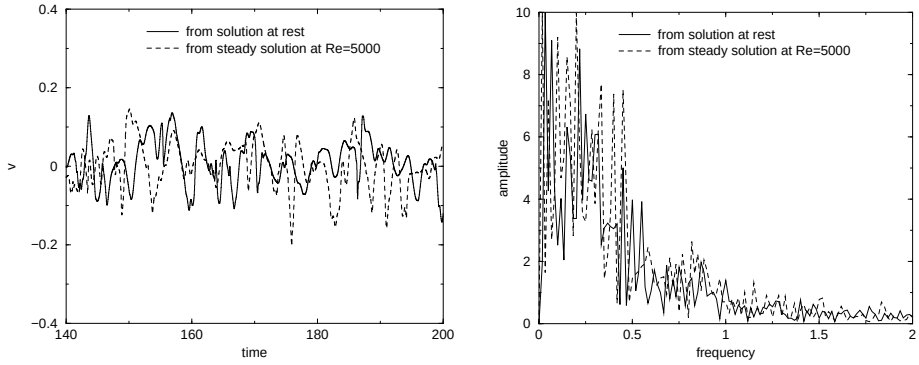

Figure 3: Zoom of vertical velocity component history (left) and power spectrum (right) at monitoring point (14/16,1/16) for $Re = 100000$.

The other numerical test of this section concerns the flow at $Re = 50000$ behind arrays of cylinders in a channel of width W (figure 4). This corresponds to a vertical soap film flow in which the driving is given by an array of horizontal cylinders and two arrays of vertical cylinders along the wall to reinforce the injection scale (see [5] and [7]). To take into account the obstacles, we use a penalization method which is equivalent to solve Darcy equations in the solid bodies [1]. On figure 4 is plotted the vorticity field for both the numerical simulation and the experiment. We see clearly that the same patterns are present in the flow although the small eddies are not easy to visualize on the picture of the experiment. To qualify these flows, we want to analyze more clearly the fully turbulent flow. To do so we store the temporal evolution of both components of the velocity at monitoring points inside the flow behind the horizontal cylinders. Fourier analysis of this temporal signals gives the power spectrum of the longitudinal and transverse components of the velocity. If the turbulence is isotropic, and if these one dimensional spectra show power law scaling, the scaling exponents can be identified with the exponents of the energy density spectrum. Recall that in two dimensional turbulence, the energy density spectrum scales as $E(k) \sim k^{-3}$ in the enstrophy cascade range ($k > k_{injection}$) while it scales as $E(k) \sim k^{-5/3}$ in the inverse energy range ($k < k_{injection}$). The results for the power spectra of the two velocity components are displayed in figure 5, where the two components have roughly equal amplitudes for most of the range of scales examined (i.e. from $W/1000$ to W) showing that the turbulence created is isotropic. Second, one can identify two different scalings of the spectra: at small scales, a scaling consistent with -3 is seen, while at larger scales, a scaling consistent with -5/3 is observed. These two ranges are located above and below $f = 40$. This frequency corresponds to 0.05W which is the diameter of the small cylinders.

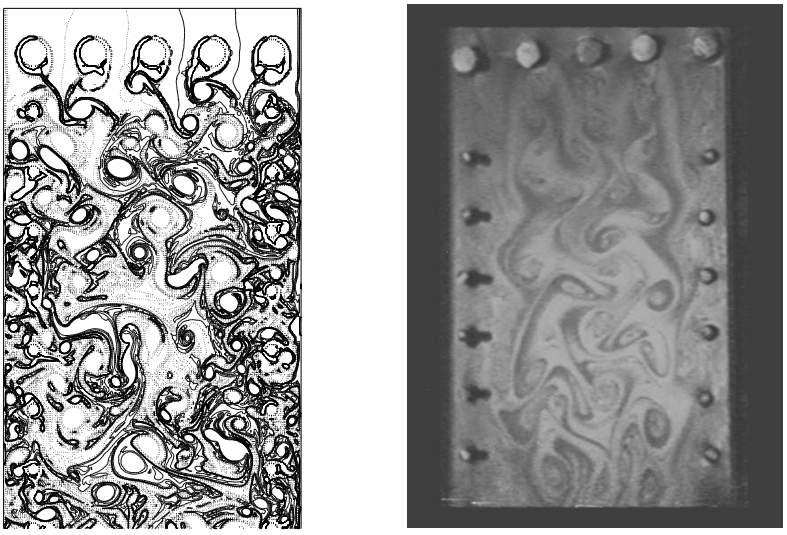

Figure 4: Vorticity field of the numerical simulation (left) and the experiment (right).

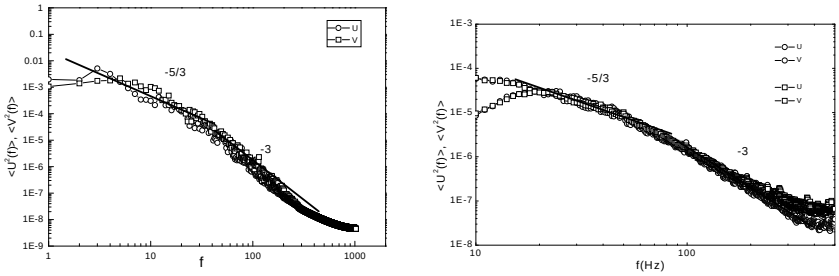

Figure 5: Velocity power spectra of the numerical simulation (left) and the experiment (right).

Conclusions

Although in 2D we can afford to perform accurate direct numerical simulations of complex incompressible flows, it is still a challenge to describe the whole behaviour of the flow with respect to the Reynolds number. In this paper, we try to shed some light on some issues that are theoretically derived for a long time: the first bifurcations, the presence of an attractor and the coexistence of the two turbulent cascades.

Reference

1. Angot Ph., Bruneau C. H. and Fabrie, P. (1999): "A penalization method to take into account obstacles in incompressible viscous flows", *Numer. Math.*, Vol 81.
2. Aston P. J. and Dellnitz M. (1999): "The computation of Lyapunov exponents via spatial integration with application to blowout bifurcations. Computational methods and bifurcation theory with applications", *Comput. Methods Appl. Mech. Eng.*, Vol. 170, *n*° 3-4.
3. Auteri F., Parolini N. and Quartapelle L. (2002): "Numerical investigation on the stability of singular driven cavity flow", *J. Comput. Phys.*, Vol. 183 *n*° 1.
4. Bruneau C. H. and Fabrie P. (1994): "Effective downstream boundary conditions for incompressible Navier-Stokes equations", *Int. J. Num. Meth. Fluids*, Vol.19 *n*° 8.
5. Bruneau C. H., Greffier O., Kellay H. (1999): "Numerical study of grid turbulence in two dimensions and comparison with experiments on turbulent soap films", *Phys. Rev. E*, Vol. 60, R1162.
6. Fortin A., Jardak M., Gervais J. J. and Pierre R. (1997): "Localization of Hopf bifurcations in fluid flow problems", *Int. J. Numer. Methods Fluids*, Vol. 24 *n*° 11.
7. Kellay H., Bruneau C. H., Wu X. L. (2000): "Probability density functions of the enstrophy flux in two dimensional grid turbulence", *Phys. Rev. Let.* Vol. 84.
8. Peng Y. F., Shiau Y. H. and Hwang R. R. (2002): "Transition in a 2-D lid-driven cavity flow", *Computers & Fluids*, Vol. 32, 337-352.
9. Sahin M. amd Owens R. G.(2003): "A novel fully-implicit finite volume method applied to the lid-driven cavity problem. Part I and II", *Int. J. Numer. Methods Fluids* Vol. 42 *n*° 1.